From a mononuclear $Fe^{II}L_2$ complex to a spin crossover $Fe^{II}_4L_6$ cage by symmetric ligand architecture modification: insights into the ammonia gas sensing mechanism

Weiyang Li,[a] Aurelian Rotaru,[b] Mariusz Wolff,[c] Serhiy Demeshko,[d] Franc Meyer,[d] Yann Garcia*[a]

[a] Institute of Condensed Matter and Nanosciences, Molecules, Solids, Reactivity (IMCN/MOST), Université catholique de Louvain, Place Louis Pasteur 1, 1348 Louvain-la-Neuve, Belgium

[b] Department of Electrical Engineering and Computer Science and MANSiD Research Center, "Stefan cel Mare" University, University Street, 13, Suceava 720229, Romania

[c] Institut für Chemische Katalyse, Universität Wien, Währinger Strasse 38, 1090 Wien, Austria

[d] Institut für Anorganische Chemie, Universität Göttingen, Tammannstrasse 4, D-37077 Göttingen, Germany

Abstract: The occurrence of spin crossover usually induces different outputs, one of which is the colour change, an essential parameter for a colorimetric sensor. Herein, by symmetric modification of the ligand architecture, two complexes: a $Fe^{II}(L1)_2$ mononuclear high-spin (HS) complex (**1**) and a $Fe^{II}_4(L2)_6$ tetranuclear spin crossover cage (**2**) were constructed as colorimetric $NH_{3(g)}$ sensors, operating in the solid state. The sensing process is accompanied by a remarkable colour change from reddish brown (**1**) or light purple (**2**) to dark grey at room temperature. **2** presents a shorter response time (90 s) to $NH_{3(g)}$ compared to **1** (8 min) due to its empty cage structure, as revealed by single crystals X-ray diffraction, and large specific surface area increasing the adsorption rate of $NH_{3(g)}$. ^{57}Fe Mössbauer spectroscopy was employed to investigate the sensing mechanism around the metal centre. A conversion of 33% Fe^{II} ions to the low-spin (LS) state was observed in **1**@NH_3, after the substitution of $NH_{3(g)}$ molecules, leading to FeN_6 sites. The sensing mechanism of **2** also involves a HS to LS transition of Fe^{II} ions induced with a new FeN_6 centre, but non-coordinated BF_4^- anions also react with NH_4^+ to form NH_4BF_4. These findings provide a foundation for exploring Fe^{II}-based coordination complexes as potential NH_3 gas sensors towards high nuclearity as well as tuneable porosity.

Keywords: Sensors; Supramolecular cages; Ammonia; Volatile organic compounds; ^{57}Fe Mössbauer spectroscopy; Spin crossover

Introduction

NH_3, as a typical environmental pollutant, is known to be produced daily in various industrial fields including chemicals production, agriculture, and manufacturing.[1] Inhalation of this toxic and irritating gas above a safe level can cause lung swelling, respiratory system injuries and even death.[2] For livestock, continuous exposure to an atmosphere containing trace amounts of $NH_{3(g)}$ will also be harmful to their growth and health.[3] Hence, the research on low-cost, high-performance and easy-to-operate $NH_{3(g)}$ sensors materials is highly needed for human health and environment protection.

Metal oxides and conjugated conducting polymers-based chemi-resistive gas sensors have been extensively investigated due to their high sensitivity and ease of fabrication.[4,5] Nevertheless, high operation temperature (150–500 °C), poor selectivity and the need for a continuous energy supply still restrict their widespread applications, *e.g.* for food quality assessment and environment monitoring.[4,5] Recently, metal organic frameworks (MOFs) materials were developed as optical NH_3 gas sensors because of their porosity as well as the diversity of metal ions.[6] For example, Zhang *et al*. developed a mixed-valence $Co^{II/III}$ MOF for highly sensitive detection of $NH_{3(g)}$ at room temperature, whereas the dual colorimetric sensing of $NH_{3(g)}$ and $H_2O_{(g)}$ molecules make this system imprecise.[7] Dinca *et al*. reported that two fluorescent MOFs can selectively detect $NH_{3(g)}$ at 100 °C, but no significant $NH_{3(g)}$ sensing selectivity was observed at room temperature.[8,9] Thus, issues like moisture stability of non-fluorescence MOFs and the high working temperature and relatively low fluorescence quantum yield of fluorescent MOFs still constrain their development.[10,11] Also, the additional instruments required for performance evaluation process such as ultraviolet-visible diffuse reflectance spectroscopy (UV-vis DRS),[7] Fourier-transform infrared (FT-IR)[12] and fluorescence spectroscopy[8,9,13] limit their use in the field. In this regard, colorimetric sensors are of great interest because of their simplicity, rapidity, powerless, visual response and ease of interpretation.[14]

In order to improve the discrimination ability of colorimetric ammonia sensors, unstable and expensive reagents are usually utilized,[15] for instance, chemochromic dyes (indophenol dyes,[16] dye 3,[17] etc.) and noble metal nanoparticles (silver,[18] gold,[19] etc.). In addition, to obtain a sensitive and reliable colorimetric sensor, the dye must be

uniformly distributed and permanently immobilized on the support medium, which makes the sensor fabrication process cumbersome and complex.[14] Furthermore, physical or chemical interactions of humidity and sensing materials can interfere with the sensing performance.[20] Good candidates for alleviating these defects are Fe^{II} coordination complexes whose spin transition (high-spin (HS)↔low-spin (LS)) is triggered by the presence of the target analyte, while the transition process may be accompanied by a colour change.[21,22] Also, some Fe^{II}-based compounds grown in aqueous solutions or mixed with water can somewhat mitigate or eliminate the effect of humidity on sensing performances. Meanwhile, Fe^{II} coordination complexes possess the intrinsic nature of being a chemosensor in that the metal ions are highly sensitive to slight changes in the surrounding coordination environments driven by guest intercalation or delamination.[23,24] For instance, Aromí *et al*. reported a nonporous Fe^{II} mononuclear complex that exhibited remarkable small-molecule sensing abilities (methanol and acetone), accompanied by a dramatic change in optical properties due to spin state switching.[25] Recently, our group developed three Fe^{II} mononuclear complexes (Scheme 1), which were able to colorimetric detect various toxic volatile chemicals under ambient conditions, but with a slow response to $NH_{3(g)}$ due to non-porosity.[26-30] The discoloration mechanism is ascribed to the substitution of coordinated water by guest $NH_{3(g)}$ molecules leading to a change in the Fe^{II} spin state from complete HS to a mixed HS/LS situation.[26-30] Notably, insight into the structural changes of the sensor from the perspective of the sensing mechanism and thus its cyclability could provide ideas for designing $NH_{3(g)}$ sensors with different applications, for example as an element of a disposable colorimetric sensor array (structural irreversibility) or as a commercial sensor for long-term use (structural reversibility). In addition, as an applicable solid state gas sensor material, good permeability is crucial, since it determines the response time and reversibility.[31] On this basis, the few successful Ln^{III} and Fe^{II}-based tetrahedral cages with cavity in solid state have been reported for $NH_{3(g)}$ sensing, but all of them are in M_4L_4 face-capped configuration.[31-33]

In order to improve the $NH_{3(g)}$ response time of Fe^{II}-based sensors as well as to investigate the sensing mechanism of different Fe^{II}-based sensors (featuring various coordination modes), we prepared here two structurally characterized complexes, namely a mononuclear HS complex **1** ($Fe^{II}L1_2(BF_4)_2$, L1 = (*E*)-2-((pyridin-2-

ylmethylene)amino)-1*H*-benzo[*de*]isoquinoline-1,3(2*H*)-dione) and a tetranuclear spin crossover (SCO) edge-bridged cage **2** ($Fe^{II}_4L2_6$, L2 = 2,7-bis(((*E*)-pyridin-2-ylmethylene)amino)benzo[lmn][3,8]phenanthroline-1,3,6,8(2*H*,7*H*) tetraone) by symmetric modification of the ligand structure (Scheme 1). Cage **2** exhibits a faster response to $NH_{3(g)}$ compared to **1** and the sensing processes for both are accompanied by distinct colour changes. **1** and cage **2** possess FeN_4O_2 and FeN_6 coordination modes provided by polydentate ligands, respectively, without the involvement of solvent molecules in the coordination, in contrast to some sensors previously reported by our group.[26-30] ^{57}Fe Mössbauer spectral data indicate that Fe^{II} ions in **1** undergo spin-state and coordination mode transitions from HS (FeN_4O_2) to LS (FeN_6). Meanwhile, a portion of Fe^{II} ions is oxidized to Fe^{III} ions leading to the sensor not being recyclable. According to the powder X-ray diffraction (PXRD) and ^{57}Fe Mössbauer spectral analysis, the sensing mechanism of cage **2** is concerned with a HS to LS transition of Fe^{II} ions caused by the new FeN_6 center and the formation of NH_4BF_4.

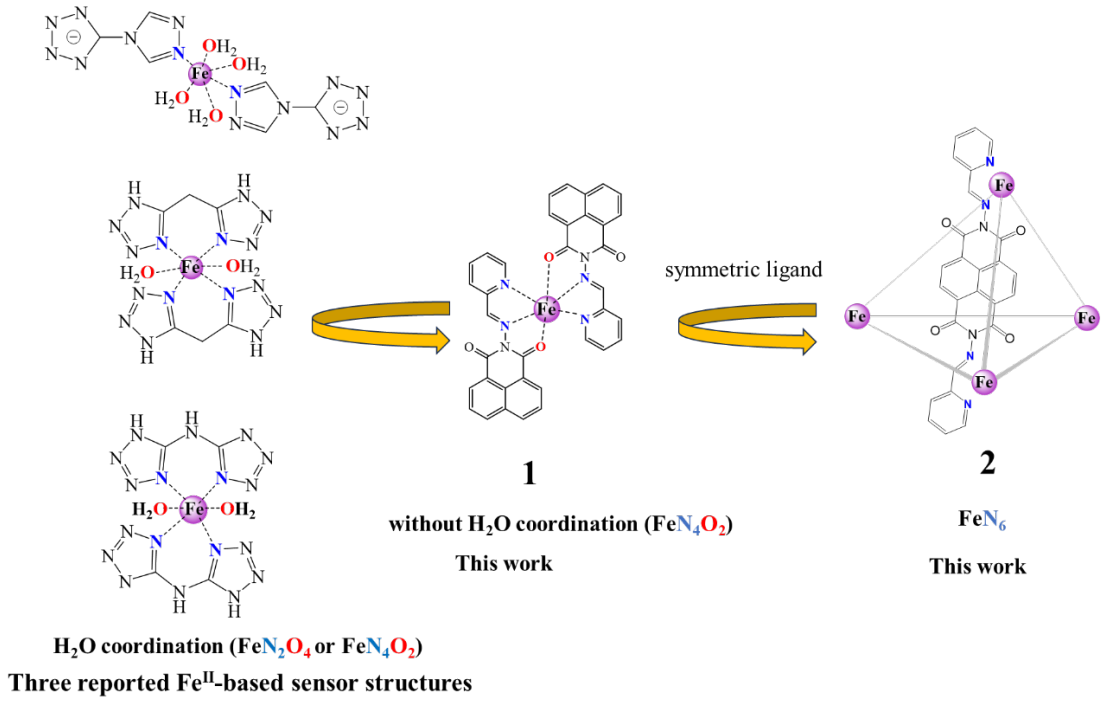

Scheme 1 Structures of three reported mononuclear Fe^{II}-based sensors,[26-30] and the newly designed Fe^{II}-based sensors (**1** and **2**).

Results and discussion

Synthesis and crystal structure of 1

N-amino-1,8-naphthalimide was synthesized through a condensation reaction between 1,8-naphthalic anhydride and hydrazine hydrate in 85% yield.[34] ^{1}H and ^{13}C NMR and high resolution mass spectra (HRMS) results confirmed the structure and purity (see ESI†). **1** was prepared via subcomponent self-assembly of *N*-amino-1,8-naphthalimide, $Fe(BF_4)_2 \cdot 6H_2O$ and 2-formylpyridine in 2 : 1 : 2 stoichiometry in acetonitrile. After filtration, diffusion of diethyl ether into the resulting purple solution over a period of two weeks produced red rod-shaped single crystals of **1**.

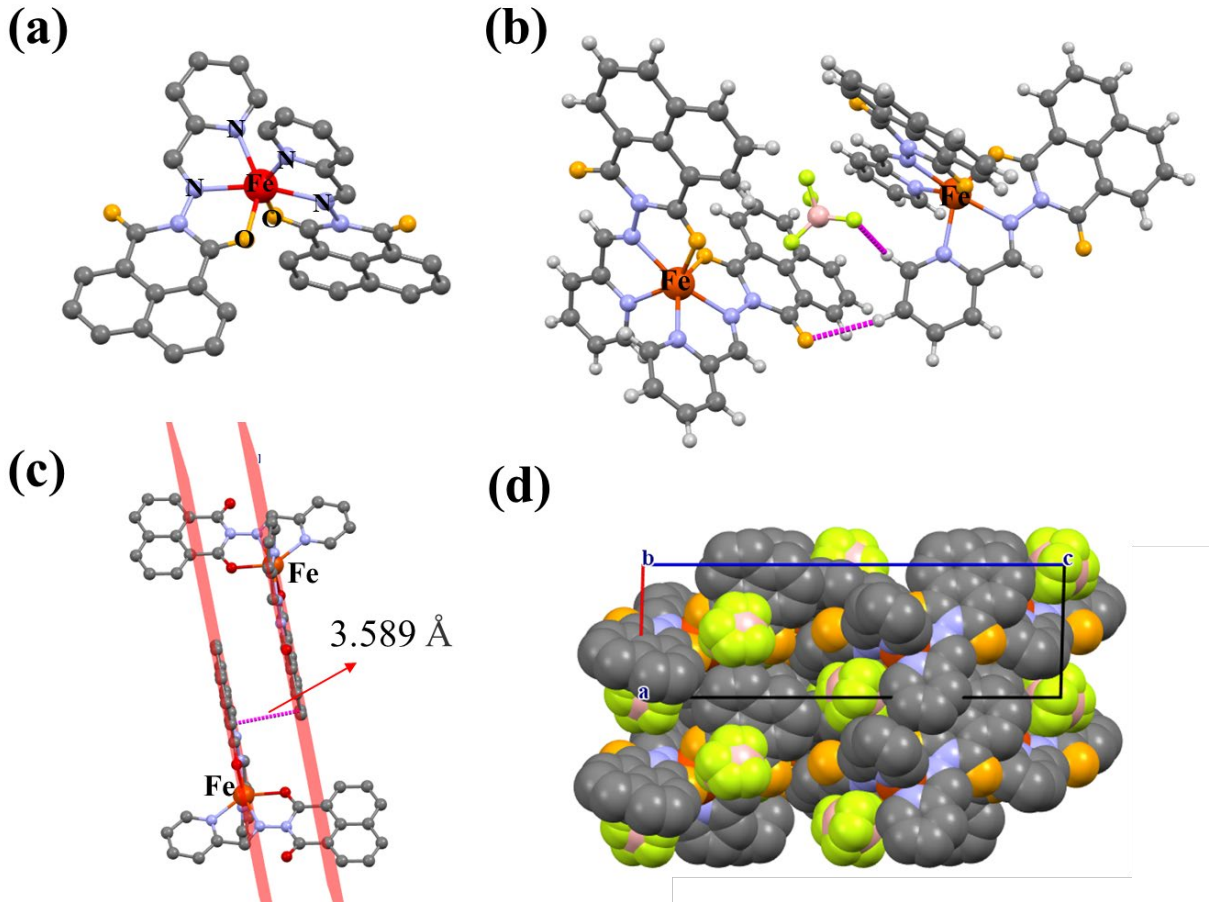

Fig. 1. (a) Coordination geometry of Fe^{II} ion in **1**. All H atoms and lattice anions have been removed for clarity; (b) Hydrogen bonding and (c) π–π interaction diagram between two adjacent molecules in **1**; (d) Spherical packing model of **1** viewed along the *b*-axis. C: dark grey; N: light blue; Fe: red; O: orange; B: pink; F: yellow.

Single crystal X-ray diffraction analysis at 120 K shows that **1** crystallizes in the monoclinic $P2_1/c$ space group with a unit cell volume of 3446.04(12) $Å^3$ (Z = 4).

Detailed crystallographic data are listed in Table S1. As shown in Fig. 1a, the Fe^{II} centre is surrounded by two tridentate ligands and adopts an N_4O_2 octahedral coordination configuration. Two BF_4^- anions are decorated around the $[Fe^{II}L1_2]^{2+}$ cations but no lattice solvents molecules were detected. Weak C−H···O and C−H···F interactions and π-π stacking interactions between adjacent aromatic rings (3.589 Å) link the molecules into a supramolecular network (Fig. 1b and 1c). However, spherical packing model for **1** shows no channels in the crystal lattice, similar to some reported Fe^{II} -based gas sensors (Fig. 1d).[26,27] The average Fe–N/O bond distances at 120 K are 2.172 Å ($Fe–N_{av}$) and 2.115 Å ($Fe–O_{av}$), typical of HS paramagnetic Fe^{II} complexes with a N_4O_2 donor set (Table S2).[27] Single crystals of **1** were also analysed at 298 K in order to follow up on whether there was a phase transition, but the crystallographic data (Table S1) did not show much difference in space group and bond distances compared to the data at 120 K. The HS state nature was further confirmed by magnetic susceptibility measurements with a room-temperature $\chi_m T$ value of 3.4 cm^3 K mol^{-1}, corresponding to pure non-interacting HS Fe^{II} species (Fig. S1).[35] Upon cooling to 25 K, the $\chi_m T$ value remains nearly constant, demonstrating that no SCO occurs. The sharp decrease observed over the range 25-2 K is due to zero-field splitting of HS Fe^{II} ions.[35]

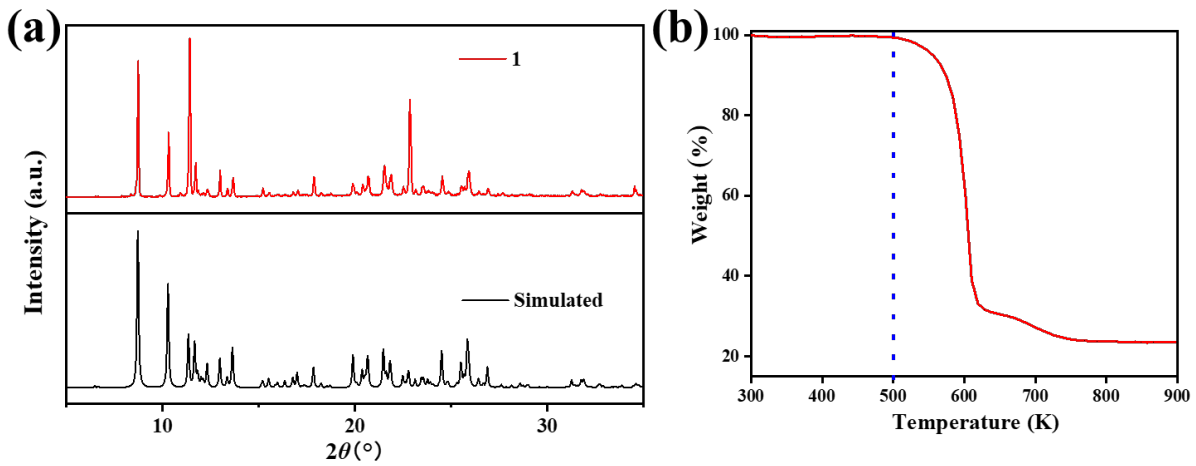

Fig. 2. (a) PXRD pattern of **1** along with the simulated pattern from single crystal XRD; (b) TGA profile of **1**.

To increase the specific surface area of the sensor, ground crystals of **1** were used in sensing experiments and the composition was confirmed by CHN analysis and HRMS (see ESI†). In addition, phase purity was confirmed by comparing powder X-ray diffraction (PXRD) pattern with the simulated diffraction peaks calculated from the

crystal structure (Fig. 2). The thermogravimetric analysis (TGA) of **1** exhibits a constant weight from 298 K to 500 K (Fig. 2), suggesting a high thermal stability compared to the reported Fe^{II}-based sensors with coordinated H_2O molecules (around 470 K).[26-30] No solvent loss was observed, which matches well with CHN results and single crystal XRD analysis. The FT-IR spectrum of **1** shows a typical stretching of pyridyl-imine groups at 1584 cm^{-1}, while the peaks near 1056 and 1014 cm^{-1} are attributed to the vibration of BF_4^- counter anions (Fig. S2).[36,37] Scanning electron microscopy energy dispersive spectroscopy (SEM-EDS) was used to study the microstructure and elemental composition. **1** showed an irregular block shape morphology (Fig. S3a). N, C, O, F, B, and Fe signals were detected in the EDS, and no impurity was observed (Fig. S3b).

1 as ammonia sensor

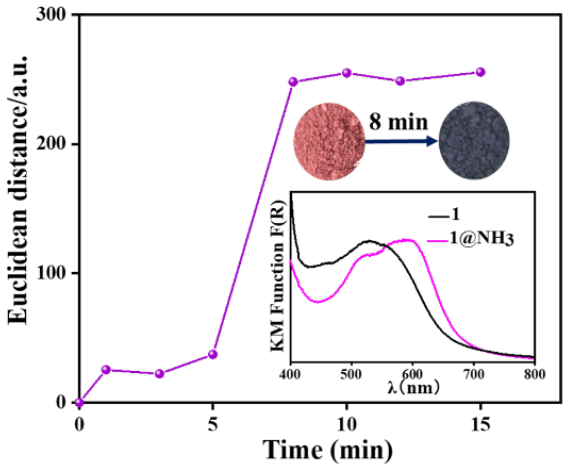

Fig. 3. Response time curve of **1** to $NH_{3(g)}$ under vapor diffusion at room temperature. Inset: diffuse reflectance spectrum and digital images of **1** and **1**@NH_3 (exposure for 8 min), KM = Kubelka-Munk.

Systems in which a colour change is evaluated with the naked eye by using a colour comparison scale are prone to errors. To quantitatively compare the colour change of **1** after exposure to $NH_{3(g)}$, we explored the conversion of colour information into numerical values, *i.e.* Euclidean distance, which is calculated based on six-dimensional colour vectors including RGB (red, green, and blue) and HSB1 (hue, saturation, and brightness) extracted from digital images taken by a smartphone.[33,38] In addition, the simple comparison of the spatial distance between the observed color and the original reference in its full original vector space is very quick and does not require sophisticated instrumentation and a tedious sample preparation process.

When the native **1** is in contact with ammonia vapor at room temperature, it turned from reddish brown to dark grey in 8 min and maintain its final colour after 15 min (Fig. 3, Fig. S4 and Table S3). The diffuse reflectance spectrum of **1** showed a broad band around λ = 535 nm, which is attributed to metal-to-ligand charge transfer (MLCT) processes.[28,29] A clear red shift of the band centred at about λ = 580 nm can be observed in **1**@NH_3, which is probably due to the $^1A_1 \rightarrow {}^1T_1$ *d*–*d* transition of the LS state of Fe^{II} ions.[28,29] Complex **1** was also separately exposed to other saturated analytes vapours including common solvents (methanol, water, acetone, etc.) and amines (hydrazine hydrate, ethanolamine, aniline, etc.), but negligible variation of the Euclidean distances was observed, indicating a good selectivity for $NH_{3(g)}$ (Fig. S5 and Table S4). In addition, the diffuse reflectance spectrum of **1**@H_2O was essentially unchanged compared to fresh **1**, further ruling out $H_2O_{(g)}$ as the cause of the colour change (Fig. S6).

Sensing mechanism of 1

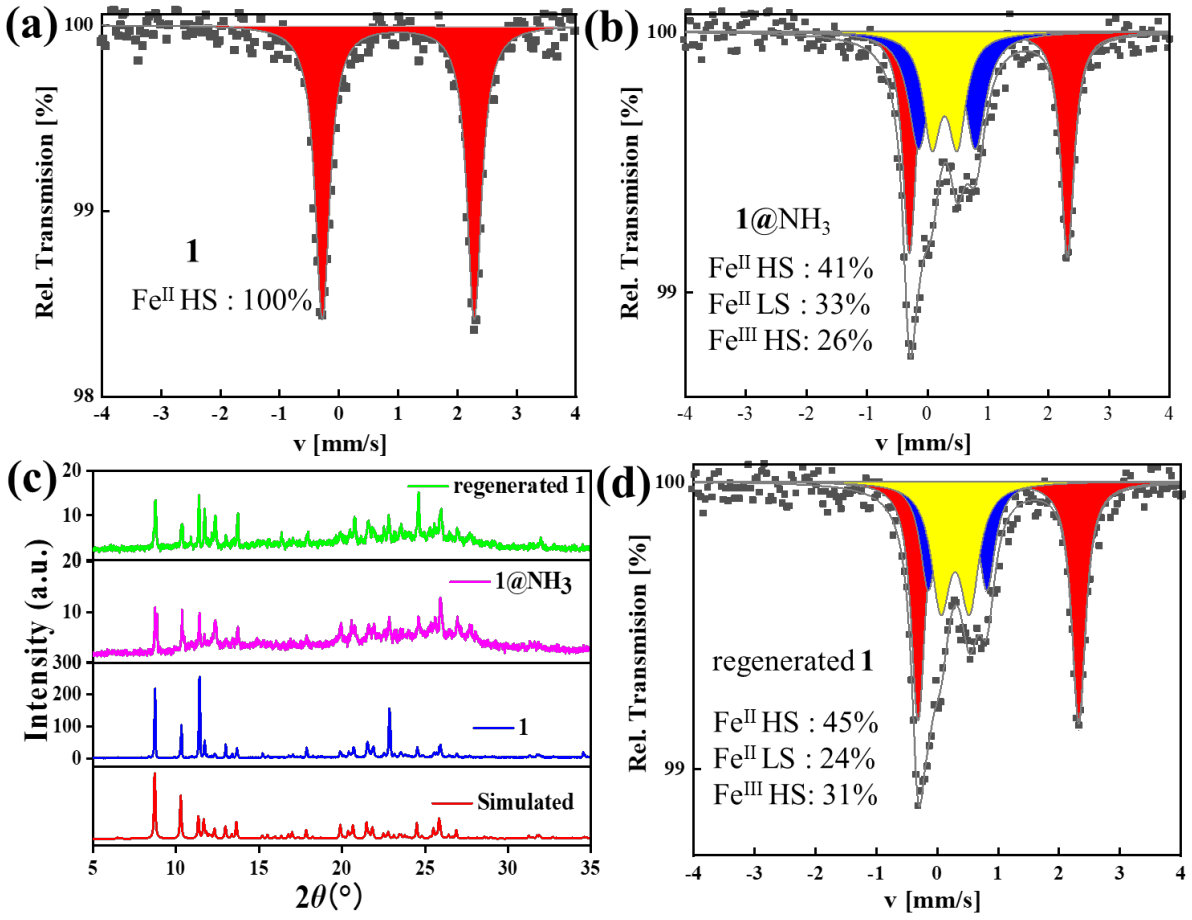

Fig. 4. ^{57}Fe Mössbauer spectra of **1** (a), **1**@NH_3 (b) and regenerated **1** (d), all recorded at room temperature and the red, blue and yellow doublets correspond to HS Fe^{II}, LS Fe^{II} and HS Fe^{III} ions, respectively; PXRD patterns of **1**, **1**@NH_3 and regenerated **1** (c).

The ^{57}Fe Mössbauer spectrum of **1** at 298 K exhibited a single doublet [isomer shift δ = 1.00(1) mm s^{-1}; quadrupole splitting ΔE_Q = 2.56(2) mm s^{-1}], corresponding to typical HS Fe^{II} ions,[39] with an area fraction (A) of 100% (Fig. 4a and Table S5). Similar Mössbauer parameters can be found in other Fe^{II} complexes with tridentate Schiff base ligands with *N*,*N*,*O* donor sets.[40-42] This result is consistent with the observations from single crystal XRD and magnetic susceptibility measurements. The slight observed asymmetry of the peaks is presumably due to a texture effect.[35] After adsorbing $NH_{3(g)}$ molecules, **1**@NH_3 displayed two new quadrupole doublets, while the original quadrupole doublet was maintained (Fig. 4b), with 41% HS Fe^{II} ions [δ = 1.00(1) mm s^{-1}; ΔE_Q = 2.61(2) mm s^{-1}], owing to the non-porous nature of **1** resulting in a gradual extension of the sensing process from the crystal surface to the interior. The doublet with blue colour in Fig. 4b [δ = 0.32(3) mm s^{-1}; ΔE_Q = 0.94(1) mm s^{-1}; A = 33%] is characteristic of LS Fe^{II} ions with a FeN_6 coordination core.[26-28] Notably, the isomer shift values agree well with those of the LS sites of reported sensors adsorbing NH_3 (δ = 0.36(3) mm s^{-1})[28] and (δ = 0.39(3) mm s^{-1}).[26] A full replacement of the coordination sphere by NH_3 molecules can be ruled out given that $[Fe(NH_3)_6]Cl_2$ and $[Fe(NH_3)_6][Fe_2(CO)_8]$ show no quadrupole splitting in their Mössbauer spectra, recorded at room temperature.[43] The other doublet with yellow colour [δ = 0.28(3) mm s^{-1}; ΔE_Q = 0.42(1) mm s^{-1}; A = 26%] is assigned to HS Fe^{III} ions,[44] presumably due to air oxidation during the sensing process. The PXRD pattern of **1**@NH_3 exhibited the characteristic peak of **1,** confirming the incomplete character of the transformation (Fig. 4c). The low diffraction intensity suggests that the new phase formed upon interaction of **1** with $NH_{3(g)}$ is amorphous. Furthermore, no thermally induced SCO behaviour was observed from the magnetic susceptibility measurement of **1**@NH_3 (Fig. S7), the lower $\chi_m T$ value (3.1 cm^3 K mol^{-1}) at 298 K being attributed to the contribution of HS Fe^{III} ions, along with the emergence of LS Fe^{II} ions. Thus, the sensing mechanism of **1** was ascribed to partial substitution of L1 by the analyte $NH_{3(g)}$ leading to a spin state conversion and partial oxidation from Fe^{II} to Fe^{III} ions. This suggests that the FeN_4O_2 coordination mode provided by the multidentate ligand L1, instead of classic water molecules,[26-30] can also undergo substitution by $NH_{3(g)}$ molecules, due to the small radius and electronegativity of the nitrogen atom compared to the oxygen atom. In

order to obtain a crystal structure after $NH_{3(g)}$ adsorption, we tried to perform sensing experiments with single crystals of **1**, but without success owing to crystals fragmentation. The cyclability was studied by heating **1**@NH_3 overnight in a vacuum at 70 °C and the resulting sample was referred to as regenerated **1**. The diffuse reflectance spectra (Fig. S8) and PXRD of regenerated **1** are in general accordance with those of **1**@NH_3, indicating that the $NH_{3(g)}$ adsorption-desorption process is irreversible. The ^{57}Fe Mössbauer spectrum of regenerated **1** exhibited a similar LS Fe^{II}: HS Fe^{II}: HS Fe^{III} (24%: 45%: 31%) ratio to that of **1**@NH_3 (33%: 41%: 26%) (Fig. 4d). We also attempted to complete the desorption process with a dilute hydrochloric acid solution, which has been reported to regenerate Fe^{II} sensors,[26,27] but **1**@NH_3 dissolved directly.

Synthesis and characterization of 2

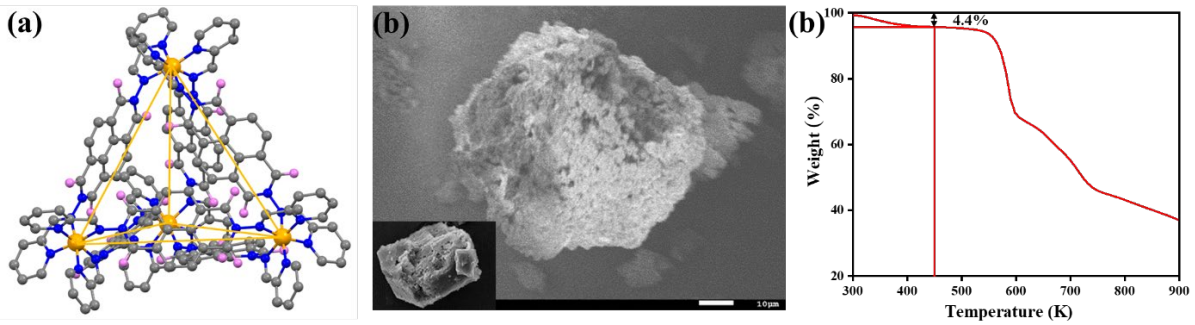

Fig. 5. (a) Crystal structure of **2** and the yellow lines connect four vertices of the Fe4 tetrahedron;[37] All H atoms and lattice anions have been removed for clarity; C: dark grey; N: blue; Fe: orange; O: violet; (b) SEM images of amorphous and crystalline[37] (inset) cage **2**; (c) TGA profile of **2**.

To improve the response time and to investigate the $NH_{3(g)}$ sensing mechanism of different Fe^{II} complex-based sensor, we designed a supramolecular cage (**2**) with FeN_6 coordination core by symmetrically modifying the ligand of **1**. Cage **2** was constructed by stirring *N*,*N*-diaminonaphthalene-1,4,5,8-tetracarboxydi-imide, 2-formylpyridine and $Fe(BF_4)_2{\cdot}6H_2O$ in a solution of CH_3CN at 65 °C under $Ar_{(g)}$ (see ESI†). Slow vapor diffusion method was used to grow single crystasl and the corresponding tetrahedron cage structure is shown in Fig. 5a.[37] Microcrystalline powder was prepared via rapid precipitation by pouring diethyl ether directly into the reaction solution. The PXRD (Fig. 7c) shows an amorphous pattern consistent with the particle clustering detected in SEM, which contrasts with the bulk morphology of cage **2** in its crystalline state[37] (Fig. 5b). The molecular formula of **2** was identified by

CHN analysis as $Fe^{II}_4L_6(BF_4)_8 \cdot 10H_2O$. The discrete tetranuclear nature was confirmed by electrospray ionization time-of-flight mass spectrometry (ESI-TOF-MS) analysis, which exhibited a series of peaks with charge states varying from 3+ to 8+ derived by the successive loss of BF_4^- counteranions (Fig. S9a). For example, peaks with *m/z* = 450.9130 correspond to $[Fe_4L_6(BF_4)]^{7+}$ species and all the observed peaks match well with the simulated isotopic patterns (Fig. S9b-S9g). The TGA curve of **2** exhibited a continuous mass loss of *ca.* 4.4% from 298 K to 450 K (Fig. 5c), which is ascribed to the release of 10 H_2O molecules, in agreement with the CHN analysis (4.6%). Above 450 K, a constant weight was observed until *ca.* 540 K, suggesting a high thermal stability, which is even higher than that of complex **1**. The FT-IR spectrum of cage **2** also exhibits absorptions for the stretching of pyridyl-imine groups (1584 cm^{-1}) and BF_4^- anions (1056 and 1014 cm^{-1}) (Fig. S10).[36,37]

Spin crossover properties of 2

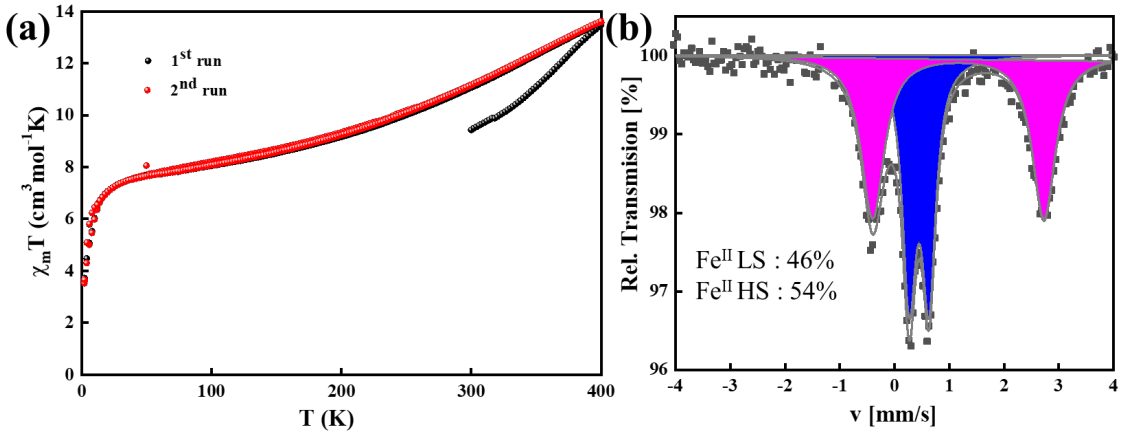

Fig. 6. (a) Plots of $\chi_m T$ vs T for cage **2**. The powder was heated from 298 K to 400 K, then annealed at 400 K in the SQUID chamber and tested in two cooling and warming cycles in the 400–2 K range; (b) ^{57}Fe Mössbauer spectrum of **2** recorded at 80 K; the blue and violet doublets correspond to LS and HS ions, respectively.

The magnetic susceptibilities of the **2** were measured over a range of 400–2 K to avoid any apparent hysteresis loops related to solvent extraction (Fig. 6a).[45] At 400 K, the $\chi_m T$ value is 13.55 cm^3 K mol^{-1}, close to the spin-only value expected for four HS Fe^{II} ions.[46] However, as the curve does not fully reach a plateau, this suggests that the SCO behaviour is incomplete and that a fraction of LS Fe^{II} ions are still present. On lowering the temperature, $\chi_m T$ progressively decreases reaching a value of 8.01 cm^3 K mol^{-1} at 80 K, which is attributed to the SCO of the Fe^{II} ion from the HS state to the

LS state. The Mössbauer spectrum recorded at 80 K (Fig. 6b and Table S6) indicates a LS/HS ratio closed to 1:1 (46 % LS and 54 % HS) and therefore the $\chi_m T$ value per one HS Fe^{II} ion can be estimated as approximately 4.0 cm^3 K mol^{-1}. Below this temperature, the sharp drop in $\chi_m T$ is due to the zero-field splitting of HS Fe^{II} ions.[35] This is confirmed by the Mössbauer measurement at 7 K (Fig. S11 and Table S6), where the LS/HS ratio remains almost the same (44 % LS and 56 % HS). Furthermore, the $\chi_m T$ vs T curve obtained in the heating mode is exactly identical to that in the cooling one, revealing no hysteresis effect. Magnetic data from the second cycle shows the same results as the first cycle. Therefore, amorphous cage **2** exhibits a gradual and incomplete spin conversion, similar to that of the crystal state,[37] which indicates that cooperative interactions accompanying the SCO process are rather weak.[47] Such SCO features have also been observed in other Fe^{II}-based polynuclear SCO compounds like tetranuclear grids and cages.[48-52]

2 as ammonia sensor

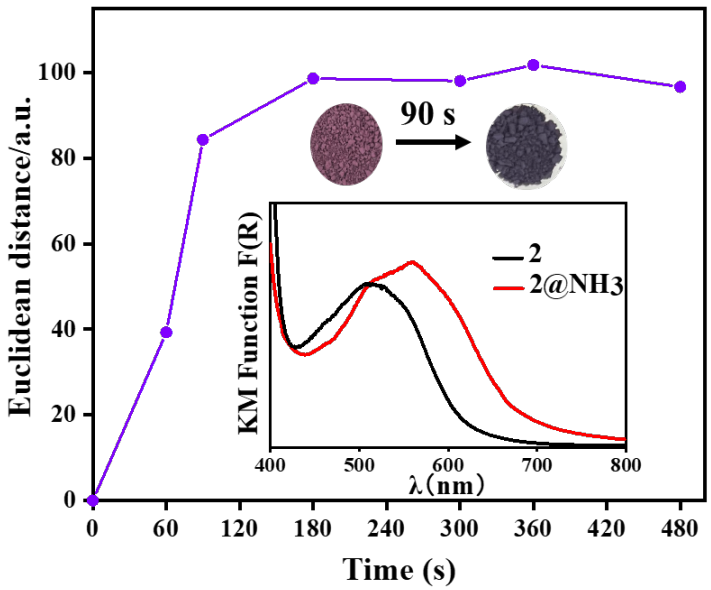

Fig. 7 Response time curve of **2** to $NH_{3(g)}$ under vapor diffusion. Inset: diffuse reflectance spectrum and digital images of **2** and **2**@NH_3, KM = Kubelka-Munk.

The sensing properties were investigated under ambient conditions based on the as-synthesized amorphous SCO cage **2**. Cage **2** was also individually exposed to different saturated analyte vapours like **1**, but only the ammonia solution was found to react with **2** (Fig. S12 and Table S7). Also, no changes in Euclidean distances and diffuse reflectance spectra (Fig. S13) were noticed in **2**@H_2O, excluding the possibility

of discoloration due to water molecules. As shown in Fig. 7, **2** can detect $NH_{3(g)}$ within 90 s and the detection process is accompanied by a clear colour variation from light purple to dark grey (shifts of optical adsorption band shown in the inset) (Table S8). The improved response speed compared to **1** (8 min) is potentially facilitated by the large specific surface area [28.16 m²/g for **2** (Fig. S14) and 8.37 m²/g for **1** (Fig. S15)], which would offer more active sites for ammonia molecules to contact, adsorb, and thus increase the response rate. In addition, the inherent cavity structure of tetrahedral cage **2** (no counter anions inside the cavity detected in the crystal structure, Fig. S16) would also increase the diffusion rate of $NH_{3(g)}$, in contrast to the nonporous nature of compound **1** (Fig. 1d).

Sensing mechanism of 2

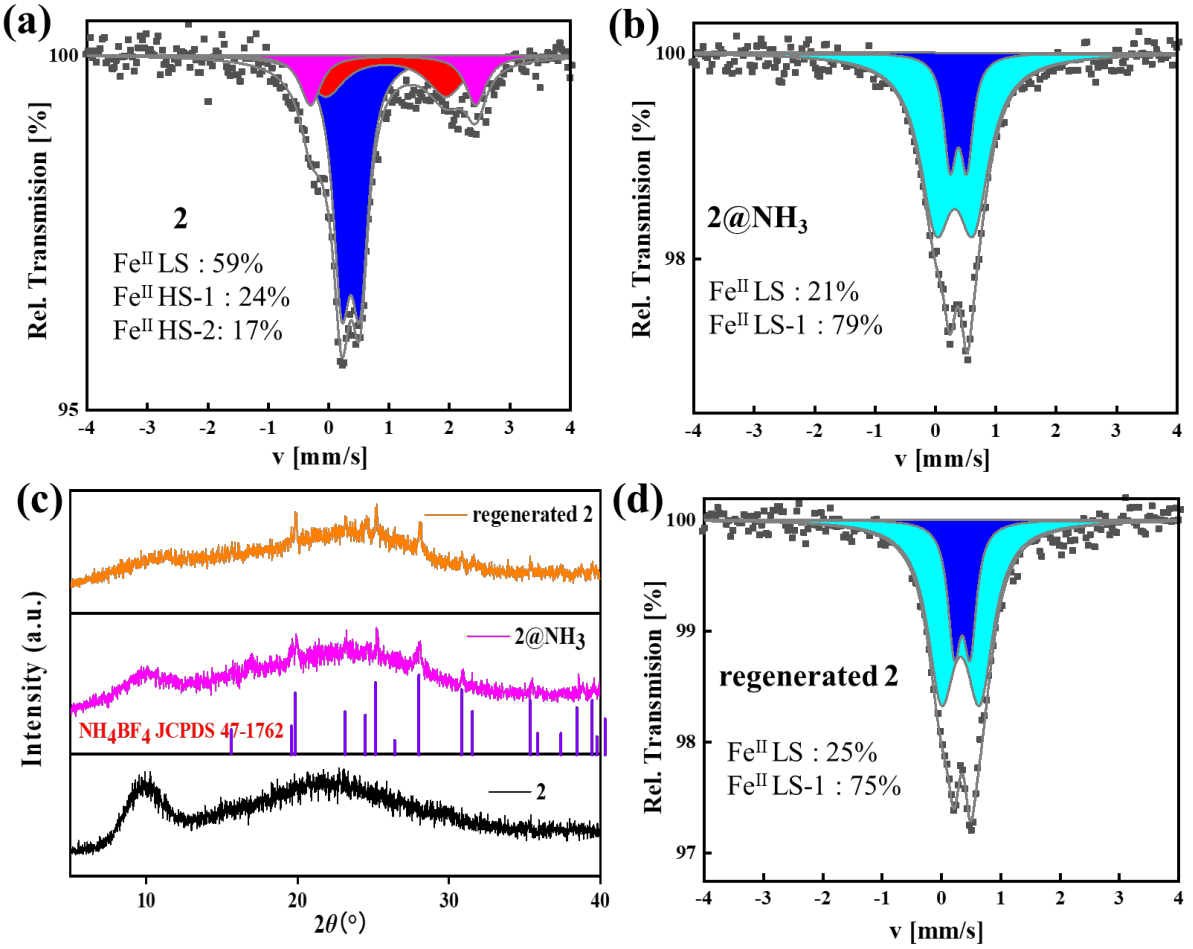

Fig. 8 ^{57}Fe Mössbauer spectra of **2** (a), **2**@NH_3 (b) and regenerated **2** (d) recorded at room temperature and the red, violet, blue and cyan doublets correspond to HS-1, HS-2, LS and LS-1 Fe^{II} ions, respectively; PXRD patterns of **2**, **2**@NH_3 and regenerated **2** (c).

^{57}Fe Mössbauer spectroscopy performed at room temperature was employed to study the sensing mechanism (Table S9). Three quadrupole doublets were identified in cage **2** (Fig. 8a). The first doublet HS-1 [δ = 0.95 mm s^{-1}; ΔE_Q = 2.00 mm s^{-1}; A = 24%] with red colour and the second doublet HS-2 [δ = 1.07 mm s^{-1}; ΔE_Q = 2.74 mm s^{-1}; A = 17%] with violet colour correspond to HS Fe^{II} ions. The third doublet with blue colour [δ = 0.37 mm s^{-1}; ΔE_Q = 0.30 mm s^{-1}; A = 59%] is assigned to LS Fe^{II} ions.[53] The LS/HS Fe^{II} ratio is 59 : 41% which at first sight seem to contradict the SQUID and Mössbauer measurements at lower temperatures, since 9.44 cm^3 K mol^{-1} at 300 K would correspond to a LS/HS ratio of 1.64 : 2.36 or 41 : 59 % (assuming 4.0 cm^3 K mol^{-1} for one HS Fe^{II} ion, see above). The reason for this is that at room temperature the Lamb-Mössbauer factor for LS Fe^{II} can be significantly higher than for HS Fe^{II}, leading to an overestimation of the fraction of LS Fe^{II} from the Mössbauer spectra.[54] Interestingly, after adsorption of $NH_{3(g)}$ molecules, **2**@NH_3 shows only two quadrupole doublets (Fig. 8b). One doublet marked by blue [δ = 0.38(2) mm s^{-1}; ΔE_Q = 0.27(3) mm s^{-1}; A = 21%] corresponds to LS Fe^{II} from **2**, however another doublet labelled in cyan LS-1 [δ = 0.32(2) mm s^{-1}; ΔE_Q = 0.62(1) mm s^{-1}; A = 79%] is also typical of LS Fe^{II}, indicating that **2** forms a new LS centre after sensing $NH_{3(g)}$ molecules. Notably, the δ and ΔE_Q values are quite similar to those LS Fe^{II} with a FeN_6 core in reported sensors, indicating that $NH_{3(g)}$ is also involved in the coordination of Fe^{II} ions.[26-28] No traces of Fe^{III} ions were detected in this Mössbauer spectrum, as Fe^{III} HS complexes usually show a quadrupole doublet with δ = 0.25–0.37 mm s^{-1} and ΔE_Q values are relatively small (<0.5 mm s^{-1}), while Fe^{III} LS complexes exhibit δ values in the range of 0.05–0.20 mm s^{-1} and relatively large ΔE_Q values of 1.9–3.0 mm s^{-1}.[44] Another possible origin of the observed LS state would be the formation of hydrogen bonds of both the imine bonds of L2 with ammonia molecules, thus modifying the electronic structure of the sensor,[55] as earlier observed in another cage compound.[33] As such, we anticipated that when heating **2**@NH_3 in a vacuum oven, a reversible transition back to the HS state would be observed. As shown in Fig. 8d, the Mössbauer spectrum of regenerated **2** exhibits two quadrupole doublets similar to **2**@NH_3: [δ = 0.35(1) mm s^{-1}; ΔE_Q = 0.27(3) mm s^{-1}; A = 25%] and [δ = 0.32(2) mm s^{-1}; ΔE_Q = 0.65(1) mm s^{-1}; A = 75%], corresponding to LS and LS-1 Fe^{II} ions. Therefore, given that heating would destroy the hydrogen bonding network, and considering that no major change in spin states and lattice sites was observed after heating, the possibility of hydrogen bonding can be ruled out. The PXRD pattern of **2**@NH_3 also exhibited amorphous humps, but

interestingly characteristic peaks of NH_4BF_4 (JCPDS 47-1762) were unambiguously identified, although $Fe(BF_4)_2{\cdot}6H_2O$ was used for the synthesis of **2**. This result indicates that $NH_{3(g)}$ and $H_2O_{(g)}$ molecules first form NH_4^+ cations, which then react with BF_4^- anions, leading to the formation of NH_4BF_4 during the sensing process (Fig. 8c). PXRD pattern, diffuse reflectance spectra (Fig. S17) and FT-IR spectral (Fig. S18) of regenerated **2** are in general agreement with those of **2**@NH_3, suggesting that the sensing process is irreversible, in line with the analysis of the ^{57}Fe Mössbauer spectra. Hence, based on the above analysis, the sensing mechanism of **2** was attributed to spin state transition of Fe^{II} ions from HS to LS (*i.e.* the formation of a new LS FeN_6 centre) upon intrusion of guest $NH_{3(g)}$ molecules, together with the formation of NH_4BF_4, a mechanism which contrasts with the one reported for another $Fe^{II}_4L_4$ cage sensor.[33] Such a difference may be related to the cage conformations and ligand structures. The reported cage features a Fe_4L_4 face-capped configuration, whereas **2** present a Fe_4L_6 edge-bridged configuration. The ligands in the reported cage are enriched in triazine functional groups, while **2** is enriched in ketone groups (O=C). Notably, triazine or nitrogen-enriched ligands can act as adsorption sites for ammonia,[7, 56] and alter the electronic structure of the sensor. Therefore, we infer that the interaction of triazine ligands with ammonia (NH···N) would be stronger than that of ketones with ammonia (NH···O=C).[57] To check this hypothesis, subcomponent ligands of **1**, **2** and the reported cage,[33] were exposed to $NH_{3(g)}$. Interestingly, the reported triazine-based ligand undergoes a colour change from bright yellow to dark yellow visible to the naked eye (which can be recovered by heating), while the subcomponent ligands of **1** and **2** do not (Fig. S19). Therefore, we infer that ammonia preferentially binds the triazine ligand during the sensing process of the reported cage,[33] whereas in the sensing process of **1** and **2**, ammonia binds the Fe^{II} ion, leading to changes in the sensor structure and thus leading to an irreversible sensing process.

Conclusions

In conclusion, two Fe^{II} complexes with different coordination spheres were synthesized via the subcomponent self-assembly. They display different sensing properties for $NH_{3(g)}$ molecules at room temperature, as well as a high thermal stability (> 500 K). The sensing process can be colorimetrically detected by a change from reddish brown (**1**) and light purple (**2**) to dark grey. **2** (90 s) exhibits a faster response than **1** (8 min) due to the presence of the cavity structure and large specific surface

area. Moreover, cage **2** also possesses excellent selectivity to $NH_{3(g)}$ among different solvents and amines. The sensing mechanism of **1** is ascribed to the substitution of O-donors of L1 by $NH_{3(g)}$ molecules and partial oxidation of Fe^{II} to Fe^{III}. This is the first example of $NH_{3(g)}$ sensor featuring a FeN_2O_4 core without any water molecules in its coordination sphere.[26-28] The sensing mechanism of **2** also differ from a recent literature report,[33] given that it involves a spin state switching from HS to LS caused by the formation of a new FeN_6 centre and the unprecedented solid-state generation of NH_4BF_4. In addition, the sensing process of $NH_{3(g)}$ is irreversible for **1** and **2**, because of the modification of the sensor structure, which is promising for applications in colorimetric sensing array technology for $NH_{3(g)}$ sensing, as most arrays are disposable.[58] Furthermore, this work provide a basis for designing and exploring new Fe^{II}-based complexes as potential NH_3 gas sensors, exploiting a variety of ligand systems, multinuclearity and porosities.

Author contributions

WL performed synthesis, characterization and wrote the manuscript with YG. AR performed SQUID and SEM measurements. MW performed ESI-TOF-HRMS experiments. SD and FM performed SQUID and some ^{57}Fe Mössbauer spectroscopic measurements.

Conflicts of interest

There are no conflicts to declare.

Acknowledgements

This work was supported through the Fonds De La Recherche Scientifique—FNRS (PDR T.0095.21, CDR J.0168.22; to Y. G.), the Ministère de l'Education et de la Recherche de Roumanie and WBI (PN-III-CEIBIM-PBE-2020-0042/8BM/2021; to Y. G. and A. R.), and the Deutsche Forschungsgemeinschaft (DFG, German Research Foundation) 217133147/SFB 1073, project B06 (to F. M.). W. Li was supported by a fellowship from the China Scholarship Council (201908310083). The authors thank Ms. Anna Fabisikova for performing mass spectrometric analyses (Mass Spectrometry Centre, University of Vienna).

References

1. D. Kwak, Y. Lei and R. Maric, *Talanta*, 2019, **204**, 713-730.
2. X. Tang, M. Debliquy, D. Lahem, Y. Yan and J. P. Raskin, *Sensors*, 2021, **21**.
3. M. Insausti, R. Timmis, R. Kinnersley and M. C. Rufino, *Sci. Total Environ.*, 2020, **706**, 135124.
4. B. Timmer, W. Olthuis and A. v. d. Berg, *Sens. Actuators B Chem.*, 2005, **107**, 666-677.
5. Z. Bielecki, T. Stacewicz, J. Smulko and J. Wojtas, *Appl. Sci*, 2020, **10**, 5111.
6. N. A. Travlou, K. Singh, E. Rodriguez-Castellon and T. J. Bandosz, *J. Mater. Chem. A*, 2015, **3**, 11417-11429.
7. J. Zhang, J. Ouyang, Y. Ye, Z. Li, Q. Lin, T. Chen, Z. Zhang and S. Xiang, *ACS Appl. Mater. Interfaces*, 2018, **10**, 27465-27471.
8. N. B. Shustova, A. F. Cozzolino, S. Reineke, M. Baldo and M. Dincă, *J. Am. Chem. Soc.*, 2013, **135**, 13326-13329.
9. M. G. Campbell, D. Sheberla, S. F. Liu, T. M. Swager and M. Dincă, *Angew. Chem. Int. Ed.*, 2015, **54**, 4349-4352.
10. S. M. Majhi, A. Ali, P. Rai, Y. E. Greish, A. Alzamly, S. G. Surya, N. Qamhieh and S. T. Mahmoud, *Nanoscale Adv.*, 2022, **4**, 697-732.
11. A. Karmakar, P. Samanta, S. Dutta and S. K. Ghosh, *Chem. Asian. J.*, 2019, **14**, 4506-4519.
12. S. Manakasettharn, A. Takahashi, T. Kawamoto, K. Noda, Y. Sugiyama and T. Nakamura, *Anal. Chem.*, 2018, **90**, 4856-4862.
13. X. Chen, Y. Yu, C. Yang, J. Yin, X. Song, J. Li and H. Fei, *ACS Appl. Mater. Interfaces*, 2021, **13**, 52765-52774.
14. A. T. Hoang, Y. B. Cho, J.-S. Park, Y. Yang and Y. S. Kim, *Sens. Actuators B Chem.*, 2016, **230**, 250-259.
15. K. J. Albert, N. S. Lewis, C. L. Schauer, G. A. Sotzing, S. E. Stitzel, T. P. Vaid and D. R. Walt, *Chem. Rev.*, 2000, **100**, 2595-2626.
16. Y. B. Cho, S. H. Jeong, H. Chun and Y. S. Kim, *Sens. Actuators B Chem.*, 2018, **256**, 167-175.
17. H. J. Oh, B. J. Yeang, Y. K. Park, H. J. Choi, J. H. Kim, Y. S. Kang, Y. Bae, J. Y. Kim, S. J. Lim, W. Lee and W. G. Hahm, *Polymers*, 2020, **12**, 1585.

18. A. Amirjani and D. H. Fatmehsari, *Talanta*, 2018, **176**, 242-246.
19. Z. Qiu, Y. Xue, J. Li, Y. Zhang, X. Liang, C. Wen, H. Gong and J. Zeng, *Chin. Chem. Lett.*, 2021, **32**, 2807-2811.
20. J. Yu, D. Wang, V. V. Tipparaju, F. Tsow and X. Xian, *ACS Sens.*, 2021, **6**, 303-320.
21. E. Resines-Urien, E. Fernandez-Bartolome, A. Martinez-Martinez, A. Gamonal, L. Piñeiro-López and J. S. Costa, *Chem. Soc. Rev.*, 2023.
22. P. Gütlich, Y. Garcia and H. A. Goodwin, *Chem. Soc. Rev.*, 2000, **29**, 419-427.
23. R. Ohtani and S. Hayami, *Chem. Eur. J.*, 2017, **23**, 2236-2248.
24. M. Steinert, B. Schneider, S. Dechert, S. Demeshko and F. Meyer, *Angew. Chem., Int. Ed.*, 2014, **126**, 6249-6253.
25. J. S. Costa, S. Rodríguez-Jiménez, G. A. Craig, B. Barth, C. M. Beavers, S. J. Teat and G. Aromí, *J. Am. Chem. Soc.*, 2014, **136**, 3869-3874.
26. L. Sun, A. Rotaru, K. Robeyns and Y. Garcia, *Ind. Eng. Chem. Res.*, 2021, **60**, 8788-8798.
27. L. Sun, A. Rotaru and Y. Garcia, *J. Hazard. Mater.*, 2022, **437**, 129364.
28. Y. Guo, S. Xue, M. M. Dîrtu and Y. Garcia, *J. Mater. Chem. C*, 2018, **6**, 3895-3900.
29. A. D. Naik, K. Robeyns, C. F. Meunier, A. F. Léonard, A. Rotaru, B. Tinant, Y. Filinchuk, B. L. Su and Y. Garcia, *Inorg. Chem.*, 2014, **53**, 1263-1265.
30. S. Xue, L. Wang, A. D. Naik, J. Oláh, K. Robeyns, A. Rotaru, Y. Guo and Y. Garcia, *Inorg. Chem. Front.*, 2021, 8, 3532–3546.
31. Y. Yao, Y. Zhou, T. Zhu, T. Gao, H. Li and P. Yan, *ACS Appl. Mater. Interfaces*, 2020, **12**, 15338-15347.
32. Y. Yao, J. Li, Y. Zhou, T. Gao, H. Li and P. Yan, *Dyes Pigm.*, 2021, **192**, 109441.
33. W. Li, L. Sun, C. Liu, A. Rotaru, K. Robeyns, M. L. Singleton and Y. Garcia, *J. Mater. Chem. C*, 2022, **10**, 9216-9221.
34. P. Raj, A. Singh, A. Singh and N. Singh, *Dalton. Trans.*, 2017, **46**, 985-994.
35. S. Xue, Y. Guo, A. Rotaru, H. Müller-Bunz, G. G. Morgan, E. Trzop, E. Collet, J. Olah and Y. Garcia, *Inorg. Chem.*, 2018, **57**, 9880-9891.
36. H. X. Zhang, X. Yan, Y. X. Chen, S. H. Zhang, T. Li, W. K. Han, L. Y. Bao, R. Shen and Z. G. Gu, *Chem. Commun.*, 2019, **55**, 1120-1123.
37. W. Li, C. Liu, J. Kfoury, J. Oláh, K. Robeyns, M. L. Singleton, S. Demeshko, F. Meyer and Y. Garcia, *Chem. Commun.*, 2022, **58**, 11653-11656.

38. P. E. Danielsson, *Comput. Graphics Image Process.*, 1980, **14**, 227-248.
39. P. Gütlich and Y. Garcia, in *Mössbauer Spectroscopy*, Springer, 2013, 23-89.
40. W. Phonsri, D. S. Macedo, K. R. Vignesh, G. Rajaraman, C. G. Davies, G. N. Jameson, B. Moubaraki, J. S. Ward, P. E. Kruger and G. Chastanet, *Chem. Eur. J.*, 2017, **23**, 7052-7065.
41. L. Zhang, G. C. Xu, H. B. Xu, V. Mereacre, Z. M. Wang, A. K. Powell and S. Gao, *Dalton. Trans.*, 2010, **39**, 4856-4868.
42. J. Yuan, S. Q. Wu, M. J. Liu, O. Sato and H. Z. Kou, *J. Am. Chem. Soc.*, 2018, **140**, 9426-9433.42.
43. G. Bancroft, M. Mays and B. Prater, *Chem. Phys. Lett.*, 1969, **4**, 248-250.
44. M. Nihei, T. Shiga, Y. Maeda and H. Oshio, *Coord. Chem. Rev.*, 2007, **251**, 2606-2621.
45. Y. Garcia, P. J. Van Koningsbruggen, E. Codjovi, R. Lapouyade, O. Kahn and L. Rabardel, *J. Mater. Chem.*, 1997, **7**, 857-858.
46. Z. Wang, L. P. Zhou, L. X. Cai, C. B. Tian and Q. F. Sun, *Nano Res.*, 2021, **14**, 398-403.
47. P. Gütlich, A. B. Gaspar and Y. Garcia, *Beilstein J. Org. Chem.*, 2013, **9**, 342-391.
48. B. Schneider, S. Demeshko, S. Dechert and F. Meyer, *Angew. Chem. Int. Ed.*, 2010, **49**, 9274-9277.
49. B. Schneider, S. Demeshko, S. Neudeck, S. Dechert and F. Meyer, *Inorg. Chem.*, 2013, **52**, 13230-13237.
50. B. Schäfer, J. F. Greisch, I. Faus, T. Bodenstein, I. Šalitroš, O. Fuhr, K. Fink, V. Schünemann, M. M. Kappes and M. Ruben, *Angew. Chem. Int. Ed.*, 2010, 2016, **55**, 10881-10885.
51. M. Ruben, E. Breuning, J. M. Lehn, V. Ksenofontov, F. Renz, P. Gütlich and G. B. Vaughan, *Chem. Eur. J.*, 2003, **9**, 4422-4429.
52. D. H. Ren, D. Qiu, C. Y. Pang, Z. Li and Z. G. Gu, *Chem. Commun.*, 2015, **51**, 788-791.
53. M. Nihei, M. Ui, M. Yokota, L. Han, A. Maeda, H. Kishida, H. Okamoto and H. Oshio, *Angew. Chem. Int. Ed.*, 2005, **117**, 6642-6645.
54. P. Gütlich, E. Bill and A. X. Trautwein, *Mössbauer spectroscopy and transition metal chemistry: fundamentals and applications*, Springer Science & Business Media, 2010.

55. F. Niu, Z. W. Shao, J. L. Zhu, L. M. Tao and Y. Ding, *J. Mater. Chem. C*, 2021, **9**, 8562-8569.
56. F. Niu, Z. W. Shao, L. M. Tao and Y. Ding, *Sens. Actuators B Chem.*, 2020, **321**, 128513.
57. G. J. Jeffrey, *An Introduction to Hydrogen Bonding*, Oxford University Press, New York, 1997.
58. J. R. Askim, M. Mahmoudi and K. S. Suslick, *Chem. Soc. Rev.*, 2013, **42**, 8649-8682.